Chinese Chemical Letters 35 (2024) 109360

Contents lists available at ScienceDirect

Chinese Chemical Letters

journal homepage: www.elsevier.com/locate/cclet

# Achieving tunable long persistent luminescence in metal organic halides based on pyridine solvent

Jun-Ting Mo [a,b], Zheng Wang [a,*]

[a] College of Chemistry and Chemical Engineering, Key Laboratory of Chemical Additives for China National Light Industry, Shaanxi University of Science and Technology, Xi'an 710021, China
[b] MOE Laboratory of Bioinorganic and Synthetic Chemistry, Lehn Institute of Functional Materials, School of Chemistry, Sun Yat-sen University, Guangzhou 510275, China

ARTICLE INFO

*Article history:*
Received 16 October 2023
Revised 2 December 2023
Accepted 4 December 2023
Available online 5 December 2023

*Keywords:*
Metal organic halide
Heavy atom effect
Halogen bond
Tunable long persistent luminescence
Anti-counterfeiting

ABSTRACT

The research of long persistent luminescence (LPL) materials has yield brilliant results in many fields. However, the efforts are still needed for the regulation of the LPL performance. In this work, a series of LPL metal organic halides with rich halogen-bond interactions, Py-$CdX_2$ (X = Cl, Br, I) were synthesized through self-assembly by $CdX_2$ and pyridine solvent. The steady-state emission redshifted and phosphorescence lifetime declined as the halogen atoms are aggravated. Three halides exhibit adjustable emission from blue to green and multiple phosphorescence from green to yellow at room temperature by changing the excitation wavelengths. Surprisingly, Py-$CdX_2$ can emit the visible color-tunable LPL from green to yellow after removing different excitation sources at ambient conditions. Combing the results of theoretical calculation and experimental analysis, it is found that heavy atom effect and the rich intermolecular halogen bond help realize LPL and multiple triplet states originated from the pyridine ring and the halogens.



Long persistent luminescence (LPL) have raised particular attention among researchers for their potential uses in persistent luminescence imaging, anti-counterfeiting, information encryption, smart materials and biotherapy [1–7]. Most organic molecules cannot emit LPL effectively due to the low intersystem crossing (ISC) efficiency and weak spin-orbit coupling (SOC). In fact, researchers have achieved LPL in pure organic phosphors by introducing lone-pair electrons (*e.g.*, N, O, P, or S), thus effectively facilitating ISC according to the EI-Sayed rule [8,9]. For further improving the spin-orbit coupling and system rigidity, coordination metal ions are introduced into the luminescent system [10–14]. The LPL performance (*e.g.*, emission wavelength, lifetime and quantum efficiency) of pure organic phosphors can be potentially strengthened and tuned by the coordination assembly strategy through rational metal selection and organic molecular design.

Organic linkers commonly used in coordination systems include aromatic carboxylic acids and nitrogen heterocyclic derivatives, which are not only the building blocks of coordination assembly but also play a dominant role in generating ultra-long LPL emission. Importantly, coordination effects and intermolecular interactions can increase the rigidity of the organic linker, thereby greatly suppressing non-radiative losses and maximizing the LPL output. In 2016, Yan's group reported two kinds of $Cd^{II}$-based coordination polymers with green LPL lifetime in which up to 755 ms by choosing 1,3-benzenedicarboxylic acid and benzimidazole as the organic building blocks [15]. It was found that interlayer C–H···$\pi$ interaction and $\pi$-$\pi$ interaction increase the rigidity of organic molecules and promoted LPL emission. Halogen atoms are one of the most widely used non-metal atoms in organic and metal-organic systems since it can form the halogen-bond interactions such as C–H···X, C-X···N, X-X and C-X···$\pi$, which suppress non-radiative transitions of triplet excitons to promote LPL and modulate LPL [16–21]. In 2020, Li's group synthesized three coordination polymers with plenty of intermolecular interactions in the framework, such as Br···N, Br···C and Br···H by simultaneously bonding halogen (Cl, Br, I) and organic luminescent units to a metal source, which presents a tunable long-lived lifetime from 54.39 ms to 16.28 ms and to 1.51 ms [22]. Since purely organic LPL systems have been largely constructed and well documented over the past decade [23–26], the effective realization and tuning of LPL properties in metal-organic hybrids remains a challenge.

To avoid complicated synthesis and introduce nitrogen heteroatom to generate triplet state, in this work, a series of metal organic halide (named Py-$CdX_2$, X = Cl, Br, I) with a rich halogen-bond network were obtained by self-assembly of $CdX_2$ (X = Cl, Br, I) and available pyridine solvent under hydrothermal condition.

* Corresponding author.
*E-mail address:* wangzhengnw@126.com (Z. Wang).

https://doi.org/10.1016/j.cclet.2023.109360
1001-8417/

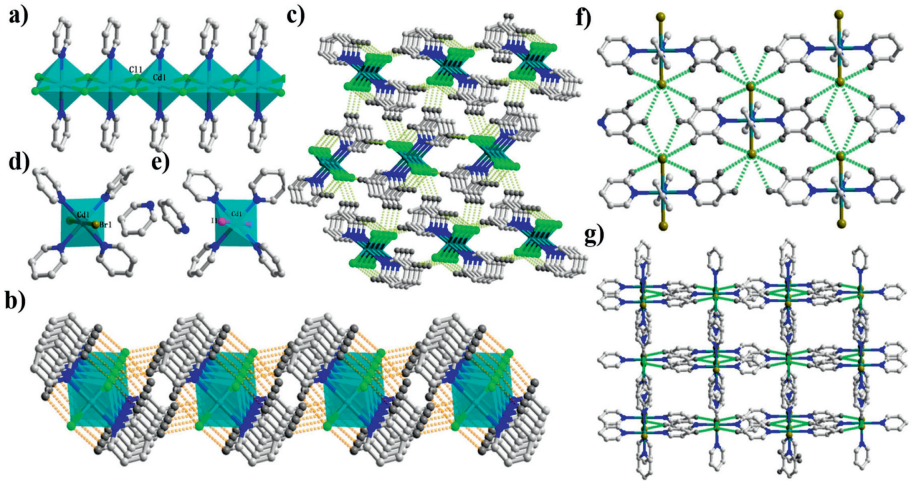


**Fig. 1.** Crystal structure of Py-$CdX_2$. (a) 1D chain structure of Py-$CdCl_2$ with 1D metal halide chain (cyan chain). (b, c) A 2D plane and a 3D network in Py-$CdCl_2$ formed through C–H···Cl interactions along the a direction and the bc plane. (d, e) 0D molecular structure of Py-$CdBr_2$ and Py-$CdI_2$. (f, g) A 2D plane and a 3D network in Py-$CdBr_2$ formed through C–H···Br interactions (all of $CdCl_4N_2$, $CdBr_2N_4$ and $CdI_2N_4$ display cyan octahedrons and hydrogen atoms are omitted for clarity).

Three halides exhibit adjustable photo-luminescence from blue to green and multiple phosphorescence from green to yellow at room temperature by changing the excitation wavelengths. More importantly, Py-$CdX_2$ successfully emit the visible color-tunable LPL from green to yellow after removing different excitation sources at ambient conditions. Combing the results of theoretical calculation and experimental analysis, it was found that heavy atom effect and the rich intermolecular halogen bond help realize LPL and multiple triplet states were produced by the pyridine and halogens.

The block crystals of Py-$CdCl_2$, Py-$CdBr_2$, and Py-$CdI_2$ were obtained in a mixture of pyridine organic solvent and the corresponding $CdX_2$ salts. Powder X-ray diffraction (PXRD) patterns of the samples exhibited excellent agreement with the simulated ones, thereby confirming the single-phase nature of the prepared products (Fig. S1 in Supporting information). The formation of the metal organic halides is also confirmed by their Fourier transform infrared spectroscopy (FT-IR) spectra (Fig. S2 in Supporting information). Thermogravimetric analysis (TGA) measurements revealed that the thermal behaviors of Py-$CdCl_2$, Py-$CdBr_2$ and Py-$CdI_2$ exhibit similarities. Their weights of the samples remain nearly constant within the temperatue range of 300–400 K, indicating their exceptional stability in ambient atmospheric conditions and ensuring the reliability of characterization and subsequent practical applications (Fig. S3 in Supporting information). Single-crystal X-ray diffraction revealed that Py-$CdCl_2$ crystallized in a monoclinic crystal sysytem $P2_1/n$ space group and corresponding crystallographic data list in Table S1 (Supporting information). The asymmetric unit consisted of half a $Cd^{2+}$ ion, one $Cl^-$ and one pyridine molecule. Of which, $Cd^{2+}$ ion displayed an twisted octahedral geometry, coordinated by four $Cl^-$ ions (Cl1, Cl1#1, Cl1#2 and Cl1#3) from metal halides and two N atoms (N1 and N1#1) from pyridine molecule (Fig. S4 in Supporting information). Interestingly, the $Cl^-$ ion played a crucial role as a $\mu_2$-Cl bridging, facilitating the connection between $Cd^{2+}$ ions to form a highly organized one-dimensional spring-like structure (Fig. 1a). The molecular stacking is significantly influenced by noncovalent intermolecular interactions, which play a crucial role in stabilizing the framework and facilitating molecular luminescence. As shown in Figs. 1b and c, a two-dimensional (2D) plane and a three-dimensional (3D) network were formed through C–H···Cl interactions along the a direction and the bc plane. Under the same synthetic condition, Py-$CdBr_2$ and Py-$CdI_2$ exhibited zero-dimensional (0D) structures due to the different radius of the halogen atom (Figs. 1d and e). Different from Py-$CdCl_2$, Py-$CdBr_2$ and Py-$CdI_2$ are isostructural and crystallized in orthorhombic crystal system with the *Ccce* space group. The asymmetric unit consisted of half a $Cd^{2+}$ ion, one $X^-$ ($Br^-$ for Py-$CdBr_2$ and $I^-$ for Py-$CdI_2$), one and a half of coordination of pyridine molecules and a half of lattice pyridine molecule. In Py-$CdBr_2$ and Py-$CdI_2$, $Cd^{2+}$ exhibited the similar coordination environment to that in Py-$CdCl_2$, where it is coordinated by four N atoms (N1, N1#1, N2 and N2#2) from pyridine molecules and two $X^-$ ions from metal salts (Br1, Br1#1 for Py-$CdBr_2$ and I1, I1#1 for $CdI_2$) (Figs. S5 and S6 in Supporting information). Similarly, inter- and intramolecular C–H···Br or C–H···I interactions assembled 0D molecule to form 2D planes and 3D networks along differents direction and planes (Figs. S5 and S6 in Supporting information). The bond lengths of Cd-N, Cd-Cl, Cd-Br, and Cd-I in these complexes range from 2.35 Å to 2.46, 2.65, 2.75 and 2.97 Å, respectively, which is similar to those of typical Cd-based complexes (Tables S2–S4 in Supporting information).

Solid-state ultraviolet (UV)–visible absorption of Py-$CdX_2$ redshifts with increasing halogen number (Fig. S7 in Supporting information). The strong absorption up to 300 nm is attributed to the $\pi$-$\pi^*$ transition of the pyridine, while the absorption at 300–350 nm is attributed to the $n$-$\pi^*$ transition. The prompt emission of Py-$CdCl_2$ was located at 420 nm with a shoulder at 470 nm under 340 nm excitation (Fig. 2a). Prompt emission of Py-$CdBr_2$ became wider and was located at 430 nm and 500 nm (Fig. 2b), while green emission dominated in Py-$CdI_2$ (Fig. 2c). As can be seen in Fig. 2d, as the halogen is aggravated, the emission red shifted from blue light to cool white light with the CIE coordinates varying from (0.26, 0.29) to (0.27, 0.31) to (0.28, 0.36). The photoluminescence (PL) quantum yield of Py-$CdCl_2$, Py-$CdBr_2$ and Py-$CdI_2$ was measured to be 6.5%, 4.9% and 3.1%, respectively decreasing with increasing halogen atomic number when excited by 340 nm wavelength at room temperature. The excitation spectra unfold an identical pattern in Py-$CdCl_2$ and Py-$CdBr_2$ with maximum peaks at 300 nm and 340 nm, while the excitation spectra of Py-$CdI_2$ narrows with maximum at 350 nm (Figs. S8–S10 in Supporting information). When excited from 260 nm to 440 nm, the prompt emission of Py-$CdX_2$ varied from the blue to yellow-green regions (Fig. S11 in Supporting information). When the excitation wavelength is around 280 nm, the Commission Internationale d'Eclairage (CIE) coordinate that appear closest to standard white light, which are (0.26, 0.33), (0.26, 0.36) and (0.28, 0.35), respectively in Py-$CdX_2$ (Table S5 in Supporting information). The time-gated spectra of Py-$CdX_2$ left at green region when delayed 1 ms (Figs. 2a–c), showing that the phosphorescence peak does not change with halogen un-

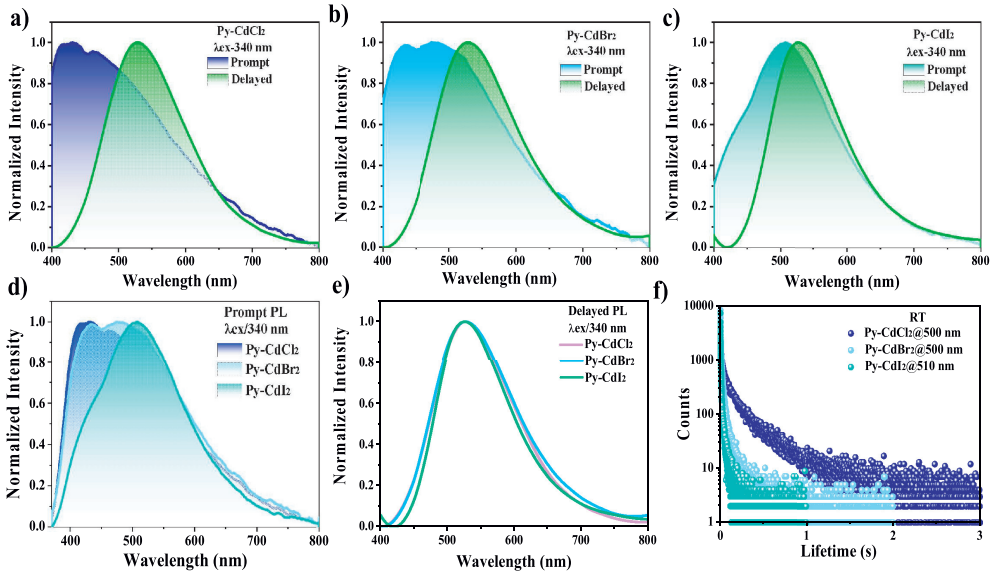


**Fig. 2.** PL properties of Py-$CdX_2$ at ambient conditions. (a–c) Prompt and delayed emission spectra. (d) Comparison of prompt emission. (e, f) Time-gated spectra and corresponding phosphorescence decay curves ($\lambda_{ex} = 340$ nm, delayed 1 ms).

der the same excitation (Fig. 2e). They are confirmed by exponential decay with a time constant of 209 ms@500 nm for Py-$CdCl_2$, 23 ms@500 nm for Py-$CdBr_2$ and 5 ms@510 nm for Py-$CdI_2$ (Fig. 2f), showing the law of significantly shorter lifetime as the halogen atom aggravated as reported in the literature [22]. The fluorescent nature in ~420 nm is also confirmed by exponential decay with a time constant of 3–9 ns for Py-$CdX_2$ (Figs. S8–S10). The prompt emission redshifted and phosphorescence lifetimes increased in the vacuum, indicating oxygen sensitivity of triplet excitons (Figs. S8–S10). Time-gated spectra and time-resolved emission spectra of Py-$CdX_2$ were virtually identically at room temperature, also demonstrating that the non-radiative deactivation of Py-$CdBr_2$ and Py-$CdI_2$ was severe, resulting in a much shorter phosphorescence lifetime (Fig. S12 in Supporting information).

To gain further insight into the phosphorescent emission of Py-$CdX_2$, temperature-dependent photoluminescence and decay curves were carried out from 300 K to 77 K (Figs. S13 and S14 in Supporting information). Emission intensities were enhanced with decreasing the temperature, while the fraction of phosphorescence in Py-$CdCl_2$ and Py-$CdBr_2$ was rapidly enhanced, so that the emission red shifted (Fig. S13b). The CIE coordinates were in the cold white light of (0.25, 0.31)@Py-$CdCl_2$, (0.26, 0.33)@Py-$CdBr_2$ and (0.28, 0.38)@Py-$CdI_2$ at 77 K (Table S6 in Supporting information). Photoluminescent decay curves in Fig. S14 showed the exponential decay ascribed to phosphorescence. At low temperatures, comparing Py-$CdBr_2$ and Py-$CdI_2$, the lifetime of Py-$CdCl_2$ increases more rapidly due to more rigid one-dimensional structure (Fig. S15 in Supporting information). The fitted phosphorescent lifetimes of Py-$CdCl_2$ are from 215 ms@300 K to 629 ms@77 K. The fitted lifetimes of Py-$CdBr_2$ and Py-$CdI_2$ are 133 ms and 17 ms at 77 K, respectively (Table S7 in Supporting information). At 77 K, the time-gated spectra under 340 nm excitation maintain the same profiles as at room temperature which implies that no new excited states appear at low temperatures (Fig. S16 in Supporting information). Considering the absorption range in UV–visible absorption spectra and the excitation spectra of halides up to 400 nm and there may be multiple emissions, excitation-dependent time-gated emission spectra of Py-$CdX_2$ were likewise collected at room temperature (Fig. S17 in Supporting information). The results show that phosphorescence can be modulated in a wide range of excitation wavelengths from 270 nm to 410 nm. Time-gated emission redshifts as the excitation wavelength grows, varying from 500 nm to 560 nm at Py-$CdCl_2$, 480 nm to 580 nm at Py-$CdBr_2$ and 490 nm to 590 nm at Py-$CdI_2$. Corresponding CIE coordinates of delayed photoluminescence spaned from green to yellow light (Table S8 in Supporting information).

Due to the excitation-dependent phosphorescent nature, five representative excitation light sources of 275, 311, 365, 385 and 405 nm were selected to collect the LPL images and time-evolved spectra of Py-$CdX_2$ (Figs. S18–S21 in Supporting information). After the flashlight is removed, the LPL spectra can be captured by the instrument, showing excitation adjustable LPL. LPL emission changed from 500 nm to 575 nm in Py-$CdCl_2$, 500 nm to 580 nm in Py-$CdBr_2$ and 530 nm to 585 nm in Py-$CdI_2$ (Figs. 3a–c). The time-evolved LPL spectra of Py-$CdCl_2$ and Py-$CdBr_2$ at 365 nm excitations are shown in Figs. 3d and e, which is optimally matched excitation wavelength. Fig. 3f shows the corresponding images of bulk sample of Py-$CdX_2$ under and after the removal of different flashlight irradiations at ambient conditions. Since the mismatch of excitation wavelengths, it is difficult for the camera to capture LPL photos after removal of 275, 311 nm excitation in Py-$CdCl_2$ and Py-$CdI_2$. However, after removing the 311 nm light, green LPL in Py-$CdBr_2$ can be observed. Yellow-green LPL in Py-$CdX_2$ can be observed with the naked eye over a duration >1 s after the removal of the 365 nm light source. As for the 385 nm and 405 nm light source, LPL color is yellow (Fig. S21 in Supporting information). The above shows that LPL color of Py-$CdX_2$ successfully changes from green to yellow in accordance with the spectral change law.

To further get insights into the mechanism of the luminescence of Py-$CdCl_2$, theoretical calculations were performed through Vienna *ab initio* simulated package (VASP). The frontier orbital analysis indicates that the highest occupied molecular orbitals (HOMO) mainly located at the chlorine atoms and pyridine ring, and the lowest unoccupied molecular orbitals (LUMO) located in the pyridine (Fig. 4a). Obviously, the halogens as heavy atoms were involved in the electronic structure and affect optical performance. This result showed that the photoemission containing singlet and triplet mainly came from the localized emission from pyridine units and charge transfer between halogens and pyridine further proving the existence of multiple triplet states. Total/partial electronic density of state (TDOS and PDOS) showed that the band gaps of Py-$CdCl_2$ is 3.30 eV and confirmed that p orbitals of the halogen participated in frontier orbitals (Fig. S22 in Supporting information).

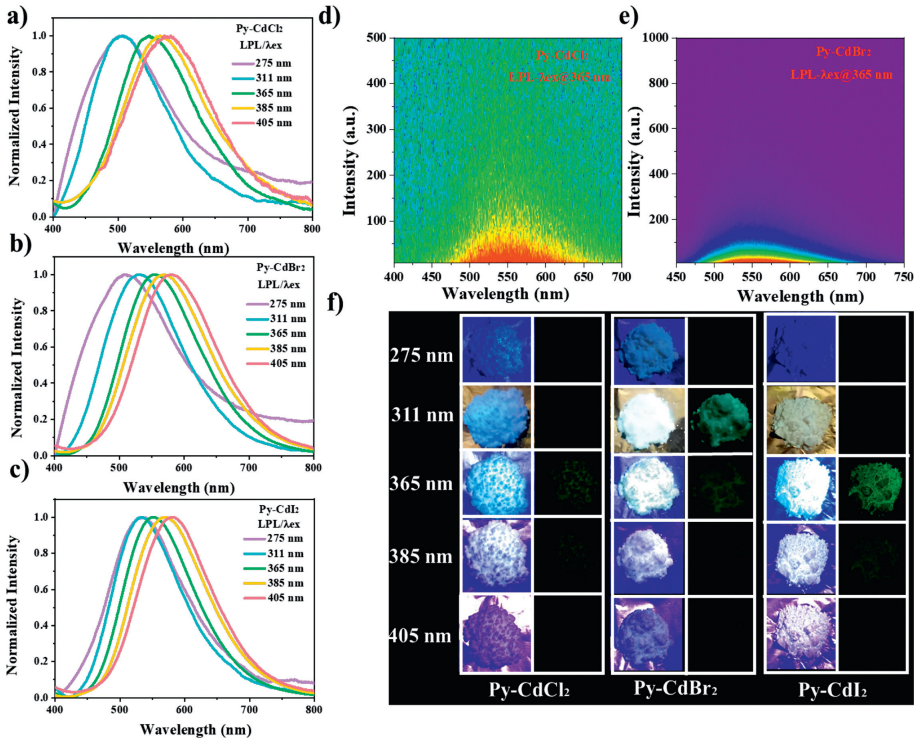


**Fig. 3.** (a–c) LPL spectra of Py-$CdX_2$ after removal of 275, 311, 365, 385 and 405 nm flashlights (collected after 8 ms). (d, e) Time evolving LPL spectra of Py-$CdCl_2$ and Py-$CdBr_2$ after removal of 365 nm excitation. (f) The LPL photos of Py-$CdX_2$ after removal of various flashlights at ambient conditions.

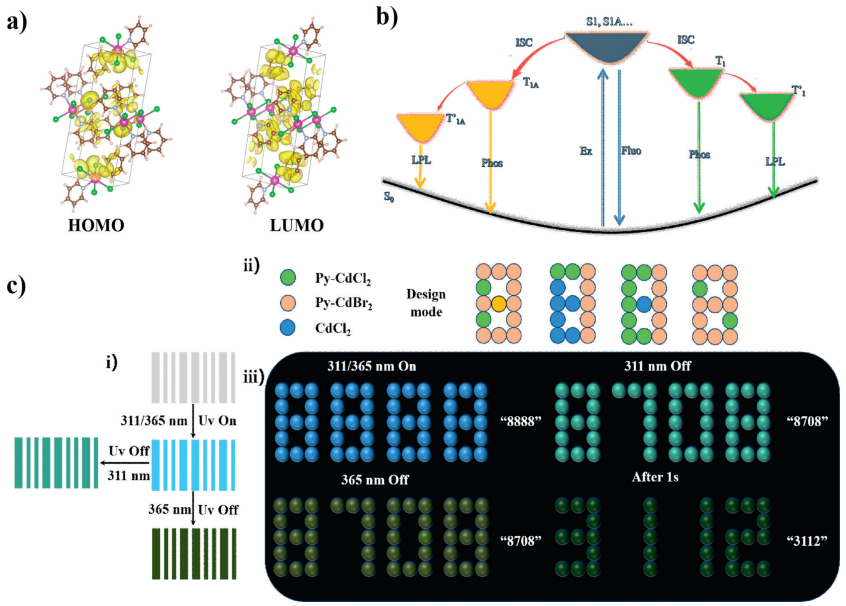


**Fig. 4.** (a) The HOMO and LUMO of Py-$CdCl_2$. (b) Jablonski diagram for LPL in the solid state. Fluo, Phos, ISC and Ex indicate fluorescence, phosphorescence, intersystem crossing, and excitation, respectively. (c) (i) The application of Py-$CdBr_2$ in the field of anti-counterfeiting. (ii) Illustration for the mode of information encryption (yellow, green and blue represent the color of the groove to differentiate colorless samples in daylight). (iii) Example of multiple encryption and decryption.

The pyridine unit crystallizes and aggregates through coordination self-assembly since the nitrogen heteroatoms are conducive to produce triplet state in the aggregation state. On the other hand, the introduction of heavy atoms increased spin orbit coupling and provided a more rigid microenvironment to hinder molecular rotation and vibration so as to stabilize the triplet excitons. Thus, the combination of heavy atoms and pyridine units enabled LPL in the aggregated state. Meanwhile, the halogen atoms induced coexistence of multiple phosphorescent peaks, realizing color tunable LPL [12].

By combination of both experimental and computational results, it is informative to uncover the mechanism of luminescence in these metal organic halides. First, the pyridine moiety in the complex absorb photon and it came to the lowest excited singlet state ($S_1$) followed by blue fluorescence (Fluo). Then, green phosphorescence (Phos, define as $P_1$) is generated through effective ISC from $S_1$ to the lowest excited triplet states ($T_1$) of the pyridine unit, while the yellow phosphorescence was generated from the triplet state ($T_{1A}$) of the aggregated state that heavy atoms involved. Next, the $T_1$ and $T_{1A}$ states relax further to the

lower-energy triplet states, leading to the green and yellow LPL (Fig. 4b). The interesting multicolor LPL properties of the material encourage us to further explore the potential applications in the field of anti-counterfeiting and information encryption. As shown in Fig. 4c(i), the " label " prepared using Py-$CdBr_2$ shows colorless in daylight. Under irradiation with 311/365 nm UV light, the "label" is blue, and when the UV light was removed, green and yellow-green LPL were exhibited, respectively. In addition, the multicolor LPL can be applied to higher level information encryption. As a proof-of-concept, a special information storage mode was designed using Py-$CdCl_2$, Py-$CdBr_2$, and $CdCl_2$ (Fig. 4c(ii)). Under 311 nm UV light, materials emit the same blue fluorescence, forming a blue "8888" pattern. Interestingly, after the UV light was turned off, Py-$CdBr_2$ continued to light, while Py-$CdCl_2$ and $CdCl_2$ were non-luminous, forming a green "8708" pattern. Furthermore, the effect of heavy atoms leads to differences in LPL duration. After removing the 365 nm UV lamp, a yellow-green "8708" pattern is formed. After 1 s, Py-$CdBr_2$ continues to emit and the LPL of Py-$CdCl_2$ disappears, thus the encrypted message is decoded as "3112" (Fig. 4c(iii)). This design has higher security, and the free combination of materials can store a large amount of encrypted information.

In summary, we utilized self-assembly of a simple and accessible solvent with $CdX_2$ (X = Cl, Br, I) to obtain LPL metal organic halides with the longest lifetime of 0.2 s at room temperature. All halides display tunable emission varied from blue to green. As expected, they successfully show excitation-dependent phosphorescence emission and LPL color varied from green to yellow. Pyridine unit, heavy atom effects and rich halogen bonding interactions produced and promoted multi- triplet states and efficient LPL. This study enriches LPL materials by simple raw materials and facile method. Such materials show great potential in applications such as information storage, encryption and anti-counterfeiting and so on.

## Declaration of competing interest

The authors declare that they have no known competing financial interests or personal relationships that could have appeared to influence the work reported in this paper.

## Acknowledgments

This research was financially supported by National Natural Science Foundation of China (No. 22101162). Start-up Foundation of Shaanxi University of Science & Technology (No. 126022036). Thanks to Dr. Meng-Yang Li of Xidian University for the computational help.

## Supplementary materials

Supplementary material associated with this article can be found, in the online version, at doi:10.1016/j.cclet.2023.109360.

## References

[1] P.Y. Fu, B.N. Li, Q.S. Zhang, et al., J. Am. Chem. Soc. 144 (2022) 2726–2734.
[2] B. Zhou, D. Yan, Chem. Sci. 13 (2022) 7429–7436.
[3] S. Yang, D. Wu, W. Gong, et al., Chem. Sci. 9 (2018) 8975–8981.
[4] Q. Huang, S. Yang, S. Feng, et al., J. Phys. Chem. Lett. 12 (2021) 1040–1045.
[5] X. Yang, D. Yan, Chem. Sci. 7 (2016) 4519–4526.
[6] B. Zhou, Z. Qi, D. Yan, Angew. Chem. Int. Ed. 61 (2022) e202208735.
[7] F. Ni, Z. Zhu, X. Tong, et al., Chem. Sci. 9 (2018) 6150–6155.
[8] N. Gan, H. Shi, Z. An, et al., Adv. Funct. Mater. 28 (2018) 1802657.
[9] A.D. Nidhankar, Goudappagouda, V.C. Wakchaure, et al., Chem. Sci. 12 (2021) 4216–4236.
[10] Z. Wang, C.Y. Zhu, S.Y. Yin, et al., Angew. Chem. Int. Ed. 58 (2019) 3481–3485.
[11] Z. Wang, C.Y. Zhu, Z.W. Wei, et al., Chem. Mater. 32 (2020) 841–848.
[12] B. Zhou, G. Xiao, D. Yan, Adv. Mater. 33 (2021) 2007571.
[13] X. Yang, D. Yan, Adv. Optical Mater. 4 (2016) 897–905.
[14] Y. Yang, K.Z. Wang, D. Yan, ACS Appl. Mater. Interfaces 8 (2016) 15489–15496.
[15] G.L. Chen, H. Feng, F.F. Feng, et al., J. Phys. Chem. Lett. 9 (2018) 6305–6311.
[16] Z. Yang, C. Xu, W.L. Li, et al., Angew. Chem. Int. Ed. 59 (2020) 17451–17455.
[17] L.J. Xu, A. Plaviak, X.S. Lin, et al., Angew. Chem. Int. Ed. 59 (2020) 23067–23071.
[18] Z. Wang, C.Y. Zhu, J.T. Mo, et al., Angew. Chem. Int. Ed. 60 (2021) 2526–2533.
[19] Y. Yang, X. Yang, X. Fang, et al., Adv. Sci. 5 (2018) 1801187.
[20] H.Y. Gao, Q.J. Shen, X.R. Zhao, et al., J. Mater. Chem. 22 (2012) 5336–5343.
[21] D.M. Guo, Y.Y. Wang, J.Z. Chen, et al., Chin. Chem. Lett. 34 (2023) 107882.
[22] Z.X. Liu, J.Q. Wang, Y. Mu, et al., Inorg. Chem. 59 (2020) 17870–17874.
[23] T.T. Wang, M. Liu, J.Y. Mao, et al., Chin. Chem. Lett. 35 (2024) 108385.
[24] S. Xu, R.F. Chen, C. Zheng, et al., Adv. Mater. 28 (2016) 9920–9940.
[25] C.R. Wang, Y.Y. Gong, W.Z. Yuan, et al., Chin. Chem. Lett. 27 (2016) 1184–1192.
[26] G.J. Qu, Y.P. Zhang, X. Ma, Chin. Chem. Lett. 30 (2019) 1809–1814.